Nonadiabatic Dynamics via the Symmetrical Quasi-Classical Method in the Presence of Anharmonicity

Alexei A. Kananenka,[†] Chang-Yu Hsieh,[‡,§] Jianshu Cao,*[,‡,§] and Eitan Geva*[]

[†]Department of Chemistry, University of Michigan, Ann Arbor, Michigan 48109, United States
[‡]Department of Chemistry, Massachusetts Institute of Technology, Cambridge, Massachusetts 02319, United States
[§]Singapore-MIT Alliance for Research and Technology (SMART) Center, Singapore 487373

Ⓢ *Supporting Information*

ABSTRACT: The symmetrical quasi-classical (SQC) method recently proposed by Miller and Cotton allows one to simulate nonadiabatic dynamics based on an algorithm with classical-like scaling with respect to system size. This is made possible by casting the electronic degrees of freedom in terms of mapping variables that can be propagated in a classical-like manner. While SQC was shown to be rather accurate when applied to benchmark models with harmonic electronic potential energy surfaces, it was also found to become inaccurate and to suffer numerical instabilities when applied to anharmonic systems. In this paper, we propose an extended SQC (E-SQC) methodology for overcoming those discrepancies by describing the anharmonic nuclear modes, which are coupled to the electronic degrees of freedom, in terms of classical-like mapping variables. The accuracy of E-SQC relative to standard SQC is demonstrated on benchmark models with quartic and Morse potential energy surfaces.
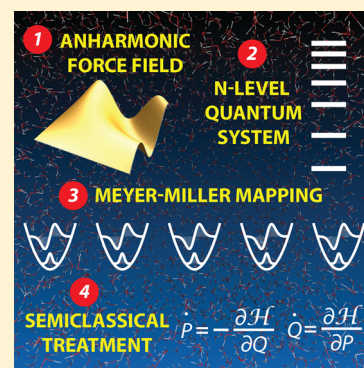
Nonadiabatic dynamics plays a central role in a variety of important chemical processes that range from electrochemistry to organic photovoltaics.[1−12] The inherently quantum nature of the underlying molecular dynamics makes simulating such processes in complex molecular systems challenging.[2,13−21] A frequently employed approximation is based on invoking linear-response to represent the nuclear degrees of freedom (DOF) in terms of uncoupled harmonic modes, and describing their coupling to the electronic DOF as linear in the normal mode coordinates.[22] The nuclear DOF and their coupling to the electronic DOF can then be described in terms of a spectral density function, which can be conveniently extracted from classical molecular dynamics (MD) simulations.[23,24] Within this framework, one can simulate the quantum-mechanically exact nonadiabatic dynamics of a system with a modest number of electronic states (up to ~10),[25−28] but only as long as the linear-response assumption remains valid.[24,29]

Despite the popularity of the aforementioned harmonic model Hamiltonians and their ability to fit many experimental observations,[30] the linear response approximation upon which they are based can break down in many systems of interest. One example is hydrogen-bonded systems.[31−43] Another example is charge transfer (CT) processes when they involve coupling to low-frequency modes and/or take place in nonpolar environments.[44] Yet another example is rate processes,[45,46] such as proton-coupled electron transfer.[47−49] In many cases of interest, the anharmonicity can be associated with a relatively small number of nuclear modes, while the remaining modes can be treated as harmonic and assumed to be linearly coupled to the anharmonic modes.[50,51]

Despite many advances in quantum-mechanically exact simulation techniques for general anharmonic Hamiltonians,[52,53] semiclassical and mixed quantum-classical approaches remain the only viable methodologies for large-scale simulations of complex technologically and biologically relevant molecular systems. Such methods include Fewest-Switches Surface-Hopping (FSSH),[54,55] the Ehrenfest method,[56] partially linearized path integral approaches,[57,58] Trotter-Based Surface-Hopping (TBSH),[59] the Forward−Backward Trajectory Solution (FBTS)[60,61] of the quantum-classical Liouville equation (QCLE),[62,63] the Linearized Semiclassical (LSC) method,[64−68] the Poisson Bracket Mapping Equation (PBME),[69−71] and the symmetrical Quasi-Classical (SQC) method.[72−78]

In this paper, we focus on the SQC method. SQC is based on the following two components: (1) mapping of the electronic DOF[79] onto classical-like variables in a manner that accounts for zero-point energy effects, while treating the nuclear DOF as classical; (2) using symmetrical window functions for initial sampling of the electronic DOF and estimation of electronic observables at later times. In a series of recent papers, Miller and Cotton have shown that SQC provides a rather accurate description of nonadiabatic dynamics,[80] can recover detailed balance,[81] can be straightforwardly applied to systems with a relatively large number of electronic states,[76] and provides a prescription for obtaining the full electronic density matrix.[77]

$$U = -\frac{Y^2}{2} + 0.1Y^4 \qquad U = -\frac{Y^2}{2} + 2Y^4 \qquad U = 15(1 - e^{-Y/2})^2 \qquad U = 2(1 - e^{-Y/2})^2$$
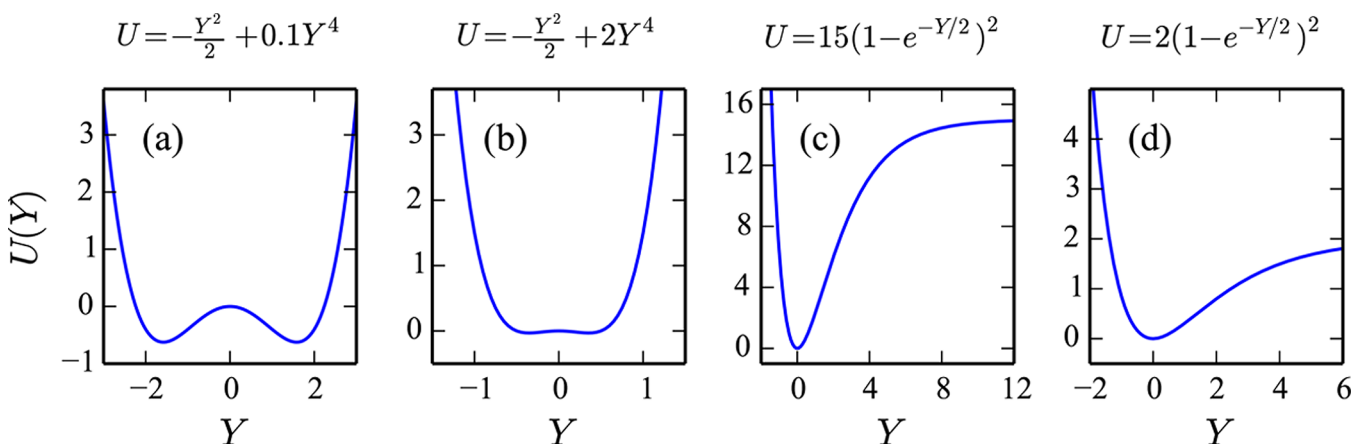
Figure 1. Primary mode anharmonic PESs studied in this work: (a) double-well quartic PES; (b) single-well quartic PES; (c) weakly anharmonic Morse PES; (d) strongly anharmonic Morse PES.

SQC's classical-like nature also implies a straightforward incorporation within standard classical MD simulation protocols.

It should be noted that usage of SQC has been far more limited than the above-mentioned competing approximate methods. This is somewhat surprising in light of the fact that SQC appears to be able to overcome several of the weaknesses that other methods suffer from. More specifically, SQC is cost-effective and scalable, is invariant to the choice of electronic basis, allows for an initially localized nuclear wavepacket to split into multiple components that are subject to different forces, and treats the electronic populations and coherences on the same footing.

The aforementioned demonstrations of SQC's accuracy were mostly based on benchmark models where the nuclear DOF are treated as harmonic. In a recent paper, Bellonzi, Jain, and Subotnik[82] have shown that adding anharmonicity to the model can cause the standard SQC approach[80] to exhibit numerical instabilities and violations of detailed balance. In this paper, we propose a way for overcoming those discrepancies. We do so by describing the anharmonic nuclear modes directly coupled to the electronic DOF in terms of classical-like mapping variables. In what follows, we show that doing so leads to a dramatic improvement in accuracy, which is robust across a wide range of anharmonicities and coupling strengths between anharmonic nuclear modes and electronic DOF.

We start out by considering a Hamiltonian of the following form:

$$\hat{H} = \hat{H}_s + \hat{H}_o + \hat{H}_{so} + \hat{H}_b + \hat{H}_{ob} \tag{1}$$

Here,

$$\hat{H}_s = \hbar\varepsilon\hat{\sigma}_z + \hbar\Delta\hat{\sigma}_x \tag{2}$$

is a two-state electronic system Hamiltonian, where $2\hbar\varepsilon$ and $\hbar\Delta$ are the electronic bias and electronic coupling between the two states, $\hat{\sigma}_z = |\uparrow\rangle\langle\uparrow| - |\downarrow\rangle\langle\downarrow|$ and $\hat{\sigma}_x = |\uparrow\rangle\langle\downarrow| + |\downarrow\rangle\langle\uparrow|$ ($|\uparrow\rangle$ and $|\downarrow\rangle$ are the electronic excited and ground states, respectively);

$$\hat{H}_o = \frac{\hat{P}_Y^2}{2M} + U(\hat{Y}) \tag{3}$$

is the Hamiltonian of the *anharmonic* primary nuclear mode directly coupled to the electronic DOF;

$$\hat{H}_b = \sum_{k=1}^{N_b} \frac{\hat{P}_k^2}{2m_k} + \sum_{k=1}^{N_b} \frac{1}{2}m_k\omega_k^2\hat{X}_k^2 \tag{4}$$

is the Hamiltonian of N_b secondary *harmonic* bath modes directly coupled to the primary mode;

$$\hat{H}_{so} = \hbar c_0\hat{Y}\hat{\sigma}_z \tag{5}$$

is the coupling Hamiltonian between the electronic system and the primary mode, where c_0 is the coupling strength;

$$\hat{H}_{ob} = -\sum_{k=1}^{N_b} c_k\hat{X}_k\hat{Y} \tag{6}$$

is the coupling Hamiltonian between the primary mode and secondary modes, where c_k is the coupling strength between the primary mode and the kth secondary mode.

It should be noted that the approach presented below is not limited to a two-state system and actually has a favorable scaling with respect to the number of electronic states. It should also be noted that our main interest in this paper is in cases where the potential energy of the primary mode, $U(\hat{Y})$, is anharmonic. In what follows, we will present results obtained for two types of anharmonic potential energy surfaces (PESs) (dimensionless variables with energy unit given by $\hbar\Delta$ and distance unit by $\sqrt{\hbar/M\Delta}$ were used):

● A quartic PES:

$$U(\hat{Y}) = -\frac{1}{2}\omega_0^2\hat{Y}^2 + \lambda\hat{Y}^4 \tag{7}$$

with $\omega_0 = 1.0$ and two different values of anharmonic coefficient λ: (i) $\lambda = 0.1$, which corresponds to a double-well PES (see Figure 1a), and (ii) $\lambda = 2.0$, which corresponds to a single-well PES (see Figure 1b).

● Morse PES:[83−85]

$$U(\hat{Y}) = D(1 - e^{-\alpha\hat{Y}})^2 \tag{8}$$

In this case, the anharmonicity can be measured by the number of bound states, $\Lambda = 2D/\omega_0$,[85] where $\omega_0 = \alpha\sqrt{2D}$ ($\Lambda \to \infty$ corresponds to the harmonic limit). Below, we report results for two different sets of parameters: (i) $D = 15.0$ and $\alpha = 0.5$, which corresponds to $\Lambda = 10$ (weakly anharmonic, see Figure 1c), and (ii) $D = 2.0$ and $\alpha = 0.5$, which corresponds to $\Lambda = 4$ (strongly anharmonic; see Figure 1d).

Within the standard SQC (S-SQC) method, the electronic operators $\{|\uparrow\rangle\langle\uparrow|, |\downarrow\rangle\langle\downarrow|, |\uparrow\rangle\langle\downarrow|, |\downarrow\rangle\langle\uparrow|\}$ are written in terms of the corresponding mapping operators:[79,86−88]

$$|j\rangle\langle k| = \frac{1}{2\hbar}(\hat{q}_j\hat{q}_k + \hat{p}_j\hat{p}_k - \gamma\hbar\delta_{jk}) \qquad (9)$$

Here, j and k are either $\uparrow$ or $\downarrow$. The optimal value of zero-point energy parameter $\gamma = 0.366$[80] was used in all calculations reported in this paper. This is followed by replacing the nuclear operators and the electronic mapping operators by their classical analogues $(\hat{q}_j \to q_j, \hat{p}_j \to p_j, \hat{Y} \to Y, \hat{P}_Y \to P_Y, \hat{X}_j \to X_j, \hat{P}_j \to P_j)$. The dynamics of $\{q_j, p_j, Y, P_Y, X_j, P_j\}$ is then governed by the corresponding classical-like counterpart of the Hamiltonian in eq 1. Initial sampling of the classical-like mapping variables, $\{q_j, p_j\}$, is based on top-hat prelimit delta function windows of width 2γ of the corresponding action variables, $n_j = (q_j^2 + p_j^2)/2\hbar - \gamma$ (angle variables are sampled randomly from $[0, 2\pi]$). More specifically, starting in state $|\uparrow\rangle$ implies that $n_\uparrow$ is a random number between $(1 - \gamma, 1 + \gamma)$ and $n_\downarrow$ is a random number between $(-\gamma, \gamma)$. The expectation values of the electronic populations at a later time are obtained using the same window functions. For example, the population of state $|\uparrow\rangle$ is determined by the fraction of trajectories with $n_\uparrow$ within $(1 - \gamma, 1 + \gamma)$ and $n_\downarrow$ within $(-\gamma, \gamma)$.

S-SQC can become inaccurate and/or numerically unstable in the presence of anharmonicity. However, as we will show below, those problems can be solved by using a methodology that we will refer to as extended SQC (E-SQC). E-SQC is based on representing $\hat{H}_{s+o} = \hat{H}_s + \hat{H}_o + \hat{H}_{so}$, rather than $\hat{H}_s$ in terms of mapping variables. More specifically, let $\{|n\rangle\}$ and $\{E_n\}$ be the eigenkets and corresponding energy levels of $\hat{H}_o$, such that

$$\hat{H}_o = \sum_{n=1}^{N} E_n|n\rangle\langle n| \qquad (10)$$

Although the number of eigenkets of $\hat{H}_o$ is in principle infinite, in practice one can obtain results at the desirable level of accuracy within a truncated basis whose size, N, can be determined by convergence (see the Supporting Information). Thus, $\{|\lambda\rangle = |\uparrow\rangle \otimes |n\rangle, |\downarrow\rangle \otimes |n\rangle\}$ form a basis for the Hilbert space of the composite system consisting of the electronic DOF and the primary mode (i.e., the Hilbert space defined by $\hat{H}_{s+o}$). Using this basis, the total Hamiltonian, eq 1, can be written as

$$\hat{H} = \sum_{\lambda\lambda'}(H_{s+o})_{\lambda\lambda'}|\lambda\rangle\langle\lambda'| + \sum_{\lambda\lambda'}(H_{ob})_{\lambda\lambda'}|\lambda\rangle\langle\lambda'| + \hat{H}_b \qquad (11)$$

It should be noted that in our truncated basis, $\hat{H}_{s+o}$ and $\hat{H}_{ob}$ are represented by $2N \times 2N$ matrices. The corresponding matrix elements of the Hamiltonian of eq 11 can be found in the Supporting Information.

In the next step, we write the operators $\{|\lambda\rangle\langle\lambda'|\}$ in terms of the corresponding mapping operators:

$$|\lambda\rangle\langle\lambda'| = \frac{1}{2\hbar}(\hat{q}_\lambda\hat{q}_{\lambda'} + \hat{p}_\lambda\hat{p}_{\lambda'} - \gamma\hbar\delta_{\lambda\lambda'}) \qquad (12)$$

Similarly to S-SQC, this is followed by replacing the bath and the mapping operators by their classical analogues $(\hat{q}_\lambda \to q_\lambda, \hat{p}_\lambda \to p_\lambda, \hat{X}_j \to X_j, \hat{P}_j \to P_j)$. The dynamics of $\{q_\lambda, p_\lambda, X_j, P_j\}$ is assumed to be governed by the classical-like Hamiltonian:

$$H_{E\text{-}SQC}(\{q_\lambda, p_\lambda\}, \{X_k, P_k\})$$
$$= \sum_{\lambda\lambda'}[(H_{s+o})_{\lambda\lambda'} + (H_{ob})_{\lambda\lambda'}]\frac{1}{2\hbar}(q_\lambda q_{\lambda'} + p_\lambda p_{\lambda'} - \gamma\hbar\delta_{\lambda\lambda'})$$
$$+ \sum_{k=1}^{N_b}\frac{P_k^2}{2m_k} + \sum_{k=1}^{N_b}\frac{1}{2}m_k\omega_k^2 X_k^2 \qquad (13)$$

E-SQC involves classical propagation of $N_b + 2N$ DOF, and is therefore computationally more demanding than S-SQC, which requires classical propagation of $N_b + 3$ DOF. However, this difference is small in the typical case where $N_b \gg N$. Furthermore, the classical-like nature of the dynamics leads to favorable scaling with the number of DOF.

We start out by considering the case where the primary mode is decoupled from the bath of secondary modes, $\hat{H}_{ob} = 0$, and for which quantum-mechanically exact results can be obtained (see the Supporting Information). The classical-like dynamics within either S-SQC or E-SQC was simulated based on the algorithm of Kelly et al.[89] with the time-step set to $\Delta t = 0.05$. All the results were obtained by averaging over 5×10^6 trajectories.

The following factorized initial density operator was used:

$$\hat{\rho}(0) = \hat{\rho}_s \otimes \hat{\rho}_o \qquad (14)$$

The electronic DOF were assumed to start out in the excited state, $\hat{\rho}_s(0) = |\uparrow\rangle\langle\uparrow|$, and the anharmonic primary mode was assumed to start out in the ground state, $\hat{\rho}_o(0) = |1\rangle\langle 1|$. Both symmetrical, $\varepsilon = 0$, and asymmetrical, $\varepsilon = 1.0$, cases were considered. E-SQC was found to perform equally well in both cases. In what follows, we only report the results for the asymmetrical case, $\varepsilon = 1.0$, which is usually considered more challenging for approximate methods.

The expectation values of $\hat{\sigma}_z$ as a function of time in the case of a primary mode with a quartic PES, as obtained from S-SQC and E-SQC, are compared to the corresponding quantum-mechanically exact results in Figure 2, for weak and strong coupling (upper and lower panels, respectively). The results show that S-SQC agrees with the exact results at short times, and starts to significantly deviate from it at longer times. The deviations are larger in the case of the double-well PES and when the coupling is strong. At the same time, E-SQC is seen to be in a very good agreement with the exact results for both single-well and double-well cases, as well as for strong and weak coupling. The size of the truncated primary mode basis, N, used to generate the results is shown at the lower right corner of each plot. In the case of a single-well PES and weak coupling $N = 2$, while in the case of a double-well PES and strong coupling $N = 6$. Thus, larger anharmonicity and stronger coupling is computationally more demanding.

The expectation values of $\hat{\sigma}_z$ as a function of time in the case of a primary mode with a Morse PES, obtained from S-SQC and E-SQC, are compared to the corresponding quantum-mechanically exact results in Figure 3, for weak and strong coupling (upper and lower panels, respectively).

Similarly to the case of the quartic PES, S-SQC is seen to agree with the exact result at short times and significantly deviate from it at longer times. The deviations are seen to increase with increasing coupling strength and degree of anharmonicity. At the same time, E-SQC is seen to be in a very good agreement with the exact results regardless of the degree of anharmonicity and coupling strength. The size of the truncated primary mode basis increases as coupling strength
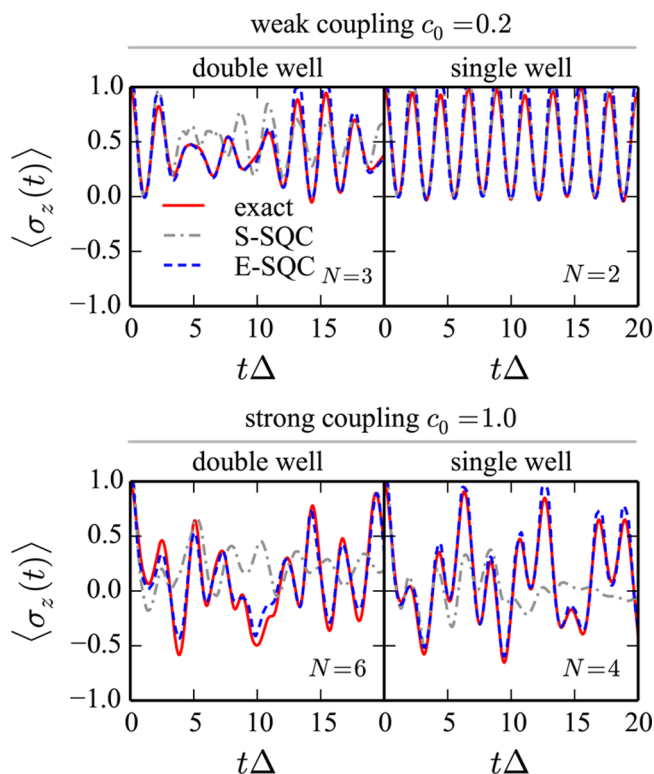
Figure 2. Expectation value $\langle \hat{\sigma}_z(t) \rangle$, as a function of time, in the case of a primary mode with double-well and single-well quartic PESs (left and right panels, respectively), as obtained from S-SQC and E-SQC, compared to the corresponding quantum-mechanically exact result, for weak and strong coupling (upper and lower panels, respectively).

Figure 3. Expectation value $\langle \hat{\sigma}_z(t) \rangle$, as a function of time, in the case of a primary mode with weakly and strongly anharmonic Morse PESs (left and right panels, respectively), as obtained from S-SQC and E-SQC, compared to the corresponding quantum-mechanically exact results, for weak and strong coupling (upper and lower panels, respectively).

changes from weak, for which $N = 2$, to strong, where $N = 4-6$. It is also seen to increase with increasing degree of anharmonicity.

It should be noted that, in the case where the primary mode is decoupled from the bath of secondary modes, $\hat{H}_{ob} = 0$, E-SQC is based on classical dynamics governed by a Hamiltonian of a quadratic form, for which one expects SQC to be more accurate. However, E-SQC also involves additional assumptions regarding initial sampling and calculating observables by binning with specific choices of the shape and width of the window functions. Thus, the deviations between the E-SQC and exact results in Figures 2 and 3 can be traced back to those additional assumptions. We next investigate the case where the anharmonic primary mode is coupled to a bath of harmonic secondary modes, $\hat{H}_{ob} \neq 0$. To this end, we consider a primary mode with a quartic PES coupled to a bath of secondary modes described by an Ohmic spectral density with exponential cutoff[22,90]

$$J(\omega) = \frac{\pi \hbar}{2} \zeta \omega e^{-\omega/\omega_c} \qquad (15)$$

Here, ζ is the Kondo parameter that measures the strength of primary–secondary mode coupling, and ω_c is the bath cutoff frequency.

The following factorized initial density operator was used:

$$\hat{\rho}(0) = \hat{\rho}_s \otimes \hat{\rho}_o \otimes \hat{\rho}_b^{eq} \qquad (16)$$

The electronic DOF were assumed to start out in the excited state, $\hat{\rho}_s(0) = |\uparrow\rangle\langle\uparrow|$. The anharmonic primary mode was assumed to start out in the ground state, $\hat{\rho}_o(0) = |1\rangle\langle1|$. The
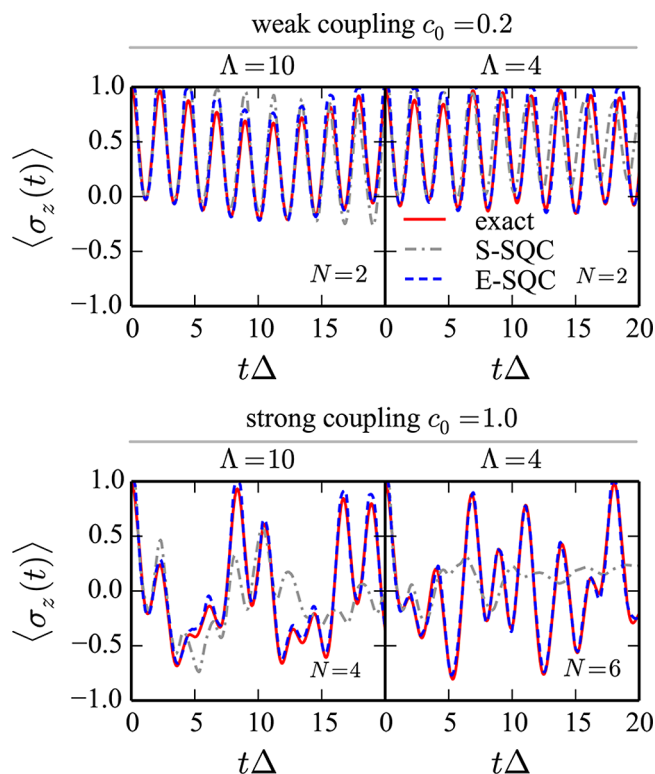
secondary bath modes were assumed to start out at thermal equilibrium, which corresponds to the following Wigner phase space density:

$$\rho_{b,W}^{eq} = \prod_{k=1}^{N_b} \frac{\tanh(\beta\omega_k/2)}{\pi} \exp\left[\frac{-2\tanh(\beta\omega_k/2)}{\omega_k} \times \left(\frac{P_k^2}{2m_k} + \frac{1}{2}m_k\omega_k^2 X_k^2 \right) \right] \qquad (17)$$

where β is the inverse temperature.

Three sets of parameters were used: (i) $\varepsilon = 0.0$, $\Delta = 0.3$, $c_0 = 0.05$, $\lambda = 0.25$, $\omega_0 = 1.2$; (ii) $\varepsilon = 0.0$, $\Delta = 0.1$, $c_0 = 0.3$, $\lambda = 0.2$, $\omega_0 = 0.6$; (iii) $\varepsilon = 0.25$, $\Delta = 0.1$, $c_0 = 0.3$, $\lambda = 0.2$, $\omega_0 = 0.6$.

The same values of the Kondo parameter, $\zeta = 0.1$, inverse temperature, $\beta = 0.2$, maximal bath mode frequency, $\omega_{max} = 3.0$, and number of secondary bath modes, $N_b = 100$, were used in all cases. Dimensionless variables were used with the energy and distance units given by $\hbar\omega_c$ and $\sqrt{\hbar/m_k\omega_c}$ for each secondary bath mode. Initial configurations of the primary and secondary modes were sampled as described in ref 51. The time step was set to $\Delta t = 0.05$ and results were averaged over 4×10^6 trajectories. It should be noted that already reasonable results can be obtained with as few as 5×10^3 trajectories (see the Supporting Information). In what follows, we compare the results obtained via E-SQC with results obtained via S-SQC, FBTS, Ehrenfest, and TBSH. It should be noted that TBSH is based on the mixed quantum-classical Liouville equation, which is expected to be the most accurate method.[91] We will therefore
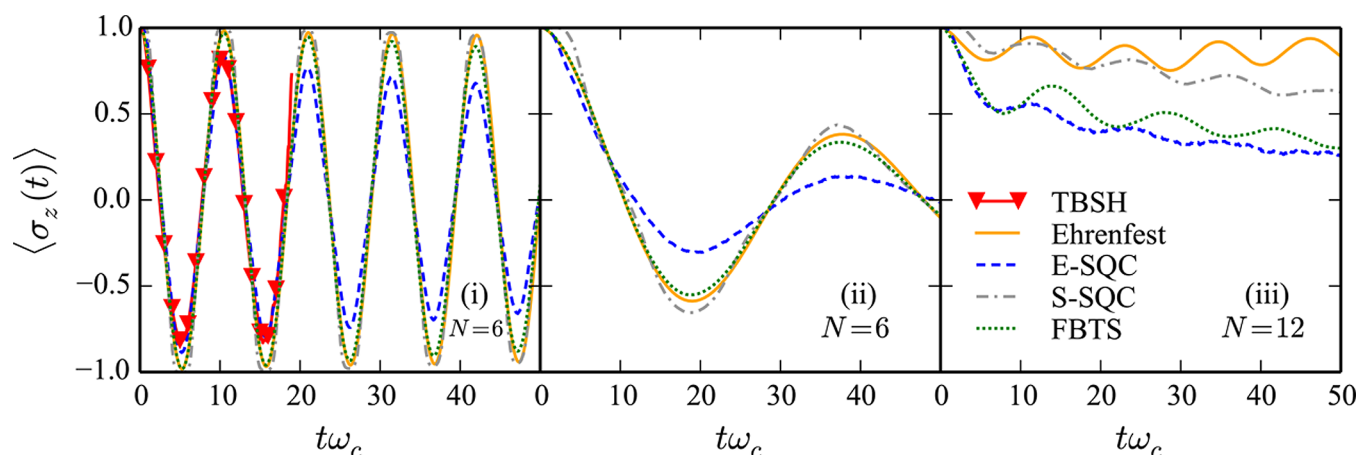
Figure 4. Expectation value $\langle \hat{\sigma}_z(t) \rangle$, as a function of time, in the case of a primary mode with a quartic PES coupled to a bath of secondary modes, for parameter sets (i), (ii), and (iii) (left, middle and right panels, respectively). Shown are the TBSH results (red solid line with red triangles), Ehrenfest results (orange solid line), E-SQC results (blue dashed line), S-SQC results (gray dash-dotted line) and FBTS results (green dotted line).

use the TBSH results as a benchmark for assessing the accuracy of the other methods.

The expectation values of $\hat{\sigma}_z$ as a function of time is shown in Figure 4 for the above-mentioned three parameter sets. The left panel corresponds to parameter set (i). The relatively large value of the diabatic coupling in this case, $\Delta = 0.3$, makes it possible to obtain TBSH results for relatively long times, $t\omega_c \approx 17$. E-SQC is seen to be in excellent agreement with TBSH in this case, which is indicative of its accuracy. It should be noted that converged E-SQC results require $N = 6$. At the same time S-SQC, FBTS and Ehrenfest are seen to deviate from TBSH. We also note that these methods appear to underdamp the oscillatory dynamics of $\langle \hat{\sigma}_z(t) \rangle$ in comparison to TBSH and E-SQC.

More pronounced differences between E-SQC and the other approximate methods are seen for parameter set (ii) (see middle panel of Figure 4). Here too, the dynamics of $\langle \hat{\sigma}_z(t) \rangle$ as predicted by S-SQC, FBTS, and Ehrenfest are seen to be underdamped compared to that predicted by E-SQC. Although TBSH is not feasible for this case, the fact that a similar trend was observed for parameter set (i) suggests that E-SQC is also more accurate in this case. Further support for this conjecture is provided in Figure 5, where we compare the exact quantum dynamics with that predicted by the various approximate methods for the same set of parameters, but in the absence of coupling to the secondary harmonic bath. While E-SQC is seen to be in a very good agreement with the quantum-mechanically exact result in this case, S-SQC, FBTS, and Ehrenfest are seen to deviate significantly from it. It should also be noted that it is unlikely that coupling to the harmonic bath is the source for the deviations, since S-SQC has been shown to be rather accurate for harmonic systems. It is therefore likely that the anharmonicity is the source of those deviations, and the results suggest that E-SQC does a better job at capturing them than S-SQC.

The results for parameter set (iii) are shown in the right panel of Figure 4. The energetic bias present in this case, $\varepsilon = 0.25$, represents a challenge for S-SQC and Ehrenfest methods. This is because Ehrenfest is known to violate detailed balance, as does S-SQC in the presence of anharmonicity.[82] However, FBTS and E-SQC are observed to capture detailed balance in this case. The fact that FBTS is underdamped compared to E-SQC also suggests that E-SQC is more accurate. As expected,
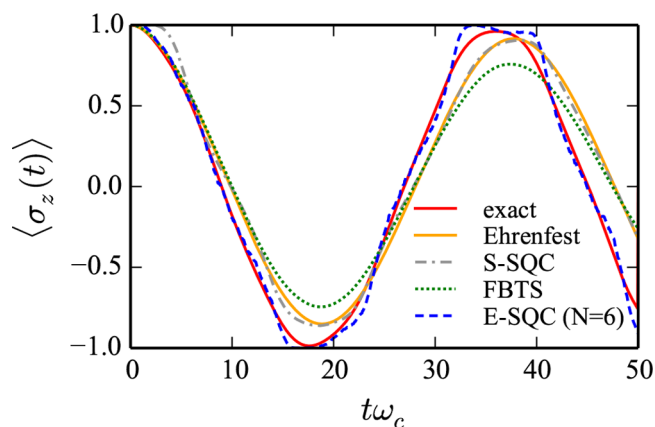

Figure 5. Expectation value $\langle \hat{\sigma}_z(t) \rangle$, as a function of time, in the case of a primary mode with a quartic PES without coupling to a bath of secondary modes, for parameter set (ii). Shown are the exact results (red solid line), Ehrenfest results (orange solid line), E-SQC results (blue dashed line), S-SQC results (gray dash-dotted line), and FBTS results (green dotted line).

the basis needed for convergence in this case, $N = 12$, is significantly larger than in the unbiased case.

Finally, we note that two general ways of verifying the convergence of E-SQC calculations with respect to the size of the truncated primary mode basis N were used in this work. Both illustrate that E-SQC is a systematically improvable method. See the Supporting Information for a detailed discussion and numerical verification of the convergence of E-SQC with respect to N.

In summary, we proposed a new methodology for overcoming inaccuracies and numerical instabilities in applications of S-SQC to anharmonic systems, which is based on describing the anharmonic nuclear modes in terms of classical-like mapping variables. The new method, which we named E-SQC, shares the advantages of S-SQC, namely, low computational cost, favorable scaling with system size, and straightforward implementation. At the same time it appears to be significantly more accurate than S-SQC in the presence of anharmonicity. E-SQC is expected to make it possible to simulate nonadiabatic dynamics in molecular systems that exhibit anharmonicity. A similar approach has been recently applied by Martinez et al. to the calculation of transient

absorption (TA) pump–probe signals using PBME and FBTS for a model system that involves harmonic PESs.[92] They illustrated that neither FBTS nor PBME was able to produce a quantitative agreement with exact population dynamics and TA signals for multiple simulation parameters irrespective of how the primary mode was treated. We showed that E-SQC is able to produce essentially exact population dynamics for a broad range of parameters. It would be highly desirable to investigate whether E-SQC can accurately describe linear and nonlinear absorption spectra for harmonic and anharmonic PESs as well. Work in this direction is underway and will be reported in future publications.

■ ASSOCIATED CONTENT

Ⓢ Supporting Information

The Supporting Information is available free of charge on the ACS Publications website at DOI: 10.1021/acs.jpclett.7b03002.

> Matrix elements of eq 11, details of exact quantum dynamics calculations and the convergence study of E-SQC methodology (PDF)

■ AUTHOR INFORMATION

Corresponding Authors

*E-mail: jianshu@mit.edu.
*E-mail: eitan@umich.edu.

ORCID Ⓞ

Alexei A. Kananenka: 0000-0001-9422-7203
Eitan Geva: 0000-0002-7935-4586

Notes

The authors declare no competing financial interest.

■ ACKNOWLEDGMENTS

■ REFERENCES

(1) Xu, D.; Schulten, K. Coupling of Protein Motion to Electron Transfer in a Photosynthetic Reaction Center: Investigating the Low Temperature Behavior in the Framework of the Spin– Boson Model. *Chem. Phys.* **1994**, *182*, 91–117.

(2) Ishizaki, A.; Fleming, G. R. Quantum Coherence in Photosynthetic Light Harvesting. *Annu. Rev. Condens. Matter Phys.* **2012**, *3*, 333–361.

(3) Liddell, P. A.; Kuciauskas, D.; Sumida, J. P.; Nash, B.; Nguyen, D.; Moore, A. L.; Moore, T. A.; Gust, D. Photoinduced Charge Separation and Charge Recombination to a Triplet State in a Carotene-Porphyrin-Fullerene Triad. *J. Am. Chem. Soc.* **1997**, *119*, 1400–1405.

(4) Liddell, P. A.; Kodis, G.; Moore, A. L.; Moore, T. A.; Gust, D. Photo Switching of Photoinduced Electron Transfer in a Dithienylethene-Porphyrin-Fullerene Triad Molecule. *J. Am. Chem. Soc.* **2002**, *124*, 7668–7669.

(5) Brédas, J.-L.; Beljonne, D.; Coropceanu, V.; Cornil, J. Charge-Transfer and Energy-Transfer Processes in π-Conjugated Oligomers and Polymers: A Molecular Picture. *Chem. Rev.* **2004**, *104*, 4971–5004.

(6) Rizzi, A. C.; van Gastel, M.; Liddell, P. A.; Palacios, R. E.; Moore, G. F.; Kodis, G.; Moore, A. L.; Moore, T. A.; Gust, D.; Braslavsky, S. E. Entropic Changes Control the Charge Separation Process in Triads Mimicking Photosynthetic Charge Separation. *J. Phys. Chem. A* **2008**, *112*, 4215–4223.

(7) Tian, H.; Yu, Z.; Hagfeldt, A.; Kloo, L.; Sun, L. Organic Redox Couples and Organic Counter Electrode for Efficient Organic Dye-Sensitized Solar Cells. *J. Am. Chem. Soc.* **2011**, *133*, 9413–9422.

(8) Mishra, A.; Fischer, M. K. R.; Bäuerle, P. Metal-Free Organic Dyes for Dye-Sensitized Solar Cells: From Structure: Property Relationships to Design Rules. *Angew. Chem., Int. Ed.* **2009**, *48*, 2474–2499.

(9) Feldt, S. M.; Gibson, E. A.; Gabrielsson, E.; Sun, L.; Boschloo, G.; Hagfeldt, A. Design of Organic Dyes and Cobalt Polypyridine Redox Mediators for High-Efficiency Dye-Sensitized Solar Cells. *J. Am. Chem. Soc.* **2010**, *132*, 16714–16724.

(10) Zhao, Y.; Liang, W. Charge Transfer in Organic Molecules for Solar Cells: Theoretical Perspective. *Chem. Soc. Rev.* **2012**, *41*, 1075–1087.

(11) Lee, M. H.; Dunietz, B. D.; Geva, E. Calculation from First Principles of Intramolecular Golden-Rule Rate Constants for Photo-Induced Electron Transfer in Molecular Donor-Acceptor Systems. *J. Phys. Chem. C* **2013**, *117*, 23391–23401.

(12) Lee, M. H.; Dunietz, B. D.; Geva, E. Donor-to-Donor vs Donor-to-Acceptor Interfacial Charge Transfer States in the Phthalocyanine-Fullerene Organic Photovoltaic System. *J. Phys. Chem. Lett.* **2014**, *5*, 3810–3816.

(13) Marcus, R. A. Chemical and Electrochemical Electron-Transfer Theory. *Annu. Rev. Phys. Chem.* **1964**, *15*, 155–196.

(14) Marcus, R. A.; Sutin, N. Electron Transfers in Chemistry and Biology. *Biochim. Biophys. Acta, Rev. Bioenerg.* **1985**, *811*, 265–322.

(15) Cukier, R. I.; Nocera, D. G. Proton-Coupled Electron Transfer. *Annu. Rev. Phys. Chem.* **1998**, *49*, 337–369.

(16) Mayer, J. M. Proton-Coupled Electron Transfer: A Reaction Chemist's View. *Annu. Rev. Phys. Chem.* **2004**, *55*, 363–390.

(17) Engel, G. S.; Calhoun, T. R.; Read, E. L.; Ahn, T.-K.; Mančal, T.; Cheng, Y.-C.; Blanken- ship, R. E.; Fleming, G. R. Evidence for Wavelike Energy Transfer Through Quantum Coherence in Photosynthetic Systems. *Nature* **2007**, *446*, 782–786.

(18) Collini, E.; Scholes, G. D. Coherent Intrachain Energy Migration in a Conjugated Polymer at Room Temperature. *Science* **2009**, *323*, 369–373.

(19) Lee, H.; Cheng, Y.-C.; Fleming, G. R. Coherence Dynamics in Photosynthesis: Protein Protection of Excitonic Coherence. *Science* **2007**, *316*, 1462–1465.

(20) Hammes-Schiffer, S.; Soudackov, A. V. Proton-Coupled Electron Transfer in Solution, Proteins, and Electrochemistry. *J. Phys. Chem. B* **2008**, *112*, 14108–14123.

(21) Worth, G. A.; Cederbaum, L. S. Beyond Born-Oppenheimer: Molecular Dynamics Through a Conical Intersection. *Annu. Rev. Phys. Chem.* **2004**, *55*, 127–158.

(22) Makri, N. The Linear Response Approximation and Its Lowest Order Corrections: An Influence Functional Approach. *J. Phys. Chem. B* **1999**, *103*, 2823–2829.

(23) Lee, M. K.; Coker, D. F. Modeling Electronic-Nuclear Interactions for Excitation Energy Transfer Processes in Light-Harvesting Complexes. *J. Phys. Chem. Lett.* **2016**, *7*, 3171–3178.

(24) Chandrasekaran, S.; Aghtar, M.; Valleau, S.; Aspuru-Guzik, A.; Kleinekathöfer, U. Influence of Force Fields and Quantum Chemistry Approach on Spectral Densities of BChl a in Solution and in FMO Proteins. *J. Phys. Chem. B* **2015**, *119*, 9995–10004.

(25) Tamura, H.; Burghardt, I.; Tsukada, M. Exciton Dissociation at Thiophene/Fullerene Interfaces: The Electronic Structures and Quantum Dynamics. *J. Phys. Chem. C* **2011**, *115*, 10205–10210.

(26) Leggett, A. J.; Chakravarty, S.; Dorsey, A. T.; Fisher, M. P. A.; Garg, A.; Zwerger, W. Dynamics of the Dissipative Two-State System. *Rev. Mod. Phys.* **1987**, *59*, 1–85.

(27) Breuer, H.-P.; Petruccione, F. *The Theory of Open Quantum Systems*; Oxford Press: Oxford, 2002.

(28) Weiss, U. *Quantum Dissipative Systems*; World Scientific: Singapore, 1999.

(29) Cao, J.; Voth, G. A. Modeling Physical Systems by Effective Harmonic Oscillators: The Optimized Quadratic Approximation. *J. Chem. Phys.* **1995**, *102*, 3337−3348.

(30) Mukamel, S. *Principles of Nonlinear Optical Spectroscopy*; Oxford University Press: New York, 1995.

(31) Sándorfy, C. Hydrogen Bonding: How Much Anharmonicity? *J. Mol. Struct.* **2006**, *790*, 50−54.

(32) Hudson, B. S.; Verdal, N. Vibrational Dynamics in Short, Strong Symmetric Hydrogen Bonds: General Considerations and Two Examples. *Phys. B* **2006**, *385*, 212−215.

(33) Hanna, G.; Geva, E. Computational Study of the One and Two Dimensional Infrared Spectra of a Vibrational Mode Strongly Coupled to Its Environment: Beyond the Cumulant and Condon Approximations. *J. Phys. Chem. B* **2008**, *112*, 12991−13004.

(34) Hanna, G.; Geva, E. Isotope Effects on the Vibrational Relaxation and Multidimensional Infrared Spectra of the Hydrogen Stretch in a Hydrogen-Bonded Complex Dissolved in a Polar Liquid. *J. Phys. Chem. B* **2008**, *112*, 15793−15800.

(35) Hanna, G.; Geva, E. Multidimensional Spectra via the Mixed Quantum-Classical Liouville Method: Signatures of Nonequilibrium Dynamics. *J. Phys. Chem. B* **2009**, *113*, 9278−9288.

(36) Hanna, G.; Geva, E. Computational Study of the Signature of Hydrogen-bond Strength on the Infrared Spectra of a Hydrogen-Bonded Complex Dissolved in a Polar Liquid. *Chem. Phys.* **2010**, *370*, 201.

(37) Hanna, G.; Geva, E. Signature of Nonadiabatic Transitions on the Pump-Probe Infrared Spectra of a Hydrogen-Bonded Complex Dissolved in a Polar Solvent: A Computational Study. *J. Phys. Chem. B* **2011**, *115*, 5191−5200.

(38) Kwac, K.; Geva, E. Mixed Quantum-Classical Molecular Dynamics Study of the Hydroxyl Stretch in Methanol/Carbon Tetrachloride Mixtures: Equilibrium Hydrogen-Bond Structure and Dynamics at the Ground State and the Infrared Absorption Spectrum. *J. Phys. Chem. B* **2011**, *115*, 9184−9194.

(39) Kwac, K.; Geva, E. Mixed Quantum-Classical Molecular Dynamics Study of the Hydroxyl Stretch in Methanol/Carbon-Tetrachloride Mixtures II: Excited State Hydrogen Bonding Structure and Dynamics, Infrared Emission Spectrum and Excited State Life-Time. *J. Phys. Chem. B* **2012**, *116*, 2856−2866.

(40) Kwac, K.; Geva, E. A Mixed Quantum-Classical Molecular Dynamics Study of the Hydroxyl Stretch in Methanol/Carbon Tetrachloride Mixtures III: Nonequilibrium Hydrogen-Bond Dynamics and Infrared Pump-Probe Spectra. *J. Phys. Chem. B* **2013**, *117*, 7737−7749.

(41) Kwac, K.; Geva, E. Solvation Dynamics of Formylperylene Dissolved in Methanol-Acetonitrile Liquid Mixtures: A Molecular Dynamics Study. *J. Phys. Chem. B* **2013**, *117*, 9996−10006.

(42) Kwac, K.; Geva, E. A Mixed Quantum-Classical Molecular Dynamics Study of anti-Tetrol and syn-Tetrol Dissolved in Liquid Chloroform: Hydrogen-Bond Structure and Its Signature on the Infrared Absorption Spectrum. *J. Phys. Chem. B* **2013**, *117*, 16493−16505.

(43) Kwac, K.; Geva, E. A Mixed Quantum-Classical Molecular Dynamics Study of anti-Tetrol and syn-Tetrol Dissolved in Liquid Chloroform II: Infrared Emission Spectra, Vibrational Excited-State Life-Times and Nonequilibrium Hydrogen-Bond Dynamics. *J. Phys. Chem. B* **2013**, *117*, 14457−14467.

(44) Wang, H.; Thoss, M. Quantum Dynamical Simulation of Electron-Transfer Reactions in an Anharmonic Environment. *J. Phys. Chem. A* **2007**, *111*, 10369−10375.

(45) Onuchic, J. N.; Beratan, D. N.; Hopfield, J. J. Some Aspects of Electron-Transfer Reaction Dynamics. *J. Phys. Chem.* **1986**, *90*, 3707−3721.

(46) Blumberger, J. Recent Advances in the Theory and Molecular Simulation of Biological Electron Transfer Reactions. *Chem. Rev.* **2015**, *115*, 11191−11238.

(47) Hammes-Schiffer, S. Theoretical Perspectives on Proton-Coupled Electron Transfer Reactions. *Acc. Chem. Res.* **2001**, *34*, 273−281.

(48) Shakib, F.; Hanna, G. Mixed Quantum-Classical Liouville Approach for Calculating Proton-Coupled Electron-Transfer Rate Constants. *J. Chem. Theory Comput.* **2016**, *12*, 3020−3029.

(49) Ananth, N.; Miller, T. F. Flux-Correlation Approach to Characterizing Reaction Pathways in Quantum Systems: a Study of Condensed-Phase Proton-Coupled Electron Transfer. *Mol. Phys.* **2012**, *110*, 1009−1015.

(50) Garg, A.; Onuchic, J. N.; Ambegaokar, V. Effect of Friction on Electron Transfer in Biomolecules. *J. Chem. Phys.* **1985**, *83*, 4491−4503.

(51) Hsieh, C.-Y.; Kapral, R. Correlation Functions in Open Quantum-Classical Systems. *Entropy* **2014**, *16*, 200−220.

(52) Meyer, H.-D.; Manthe, U.; Cederbaum, L. The Multi-Configurational Time-Dependent Hartree Approach. *Chem. Phys. Lett.* **1990**, *165*, 73−78.

(53) Wang, H. Multilayer Multiconfiguration Time-Dependent Hartree Theory. *J. Phys. Chem. A* **2015**, *119*, 7951−7965.

(54) Tully, J. C. Molecular Dynamics with Electronic Transitions. *J. Chem. Phys.* **1990**, *93*, 1061−1071.

(55) Subotnik, J. E.; Jain, A.; Landry, B.; Petit, A.; Ouyang, W.; Bellonzi, N. Understanding the Surface Hopping View of Electronic Transitions and Decoherence. *Annu. Rev. Phys. Chem.* **2016**, *67*, 387−417.

(56) McLachlan, A. A Variational Solution of the Time-Dependent Schrodinger Equation. *Mol. Phys.* **1964**, *8*, 39−44.

(57) Huo, P.; Miller, T. F., III; Coker, D. F. Communication: Predictive Partial Linearized Path Integral Simulation of Condensed Phase Electron Transfer Dynamics. *J. Chem. Phys.* **2013**, *139*, 151103.

(58) Lambert, R.; Makri, N. Quantum-Classical Path Integral. I. Classical Memory and Weak Quantum Nonlocality. *J. Chem. Phys.* **2012**, *137*, 22A552.

(59) Mac Kernan, D.; Ciccotti, G.; Kapral, R. Trotter-Based Simulation of Quantum-Classical Dynamics. *J. Phys. Chem. B* **2008**, *112*, 424−432.

(60) Hsieh, C.-Y.; Kapral, R. Nonadiabatic Dynamics in Open Quantum-Classical Systems: Forward-Backward Trajectory Solution. *J. Chem. Phys.* **2012**, *137*, 22A507.

(61) Hsieh, C.-Y.; Kapral, R. Analysis of the Forward-Backward Trajectory Solution for the Mixed Quantum-Classical Liouville Equation. *J. Chem. Phys.* **2013**, *138*, 134110.

(62) Martens, C. C.; Fang, J. Semiclassical-limit Molecular Dynamics on Multiple Electronic Surfaces. *J. Chem. Phys.* **1997**, *106*, 4918−4930.

(63) Kapral, R.; Ciccotti, G. Mixed Quantum-Classical Dynamics. *J. Chem. Phys.* **1999**, *110*, 8919−8929.

(64) Sun, X.; Geva, E. Equilibrium Fermi's Golden Rule Charge Transfer Rate Constants in the Condensed Phase: The Linearized Semiclassical Method vs Classical Marcus Theory. *J. Phys. Chem. A* **2016**, *120*, 2976−2990.

(65) Sun, X.; Geva, E. Nonequilibrium Fermi's Golden Rule Charge Transfer Rates via the Linearized Semiclassical Method. *J. Chem. Theory Comput.* **2016**, *12*, 2926−2941.

(66) Sun, X.; Geva, E. Non-Condon Equilibrium Fermi's Golden Rule Electronic Transition Rate Constants via the Linearized Semiclassical Method. *J. Chem. Phys.* **2016**, *144*, 244105.

(67) Sun, X.; Geva, E. Non-Condon Nonequilibrium Fermi's Golden Rule Rates from the Linearized Semiclassical Method. *J. Chem. Phys.* **2016**, *145*, 064109.

(68) Kananenka, A. A.; Sun, X.; Schubert, A.; Dunietz, B. D.; Geva, E. A Comparative Study of Different Methods for Calculating Electronic Transition Rates. *J. Chem. Phys.* **2018**, *148*, 102304.

(69) Kim, H.; Nassimi, A.; Kapral, R. Quantum-Classical Liouville Dynamics in the Mapping Basis. *J. Chem. Phys.* **2008**, *129*, 084102.

(70) Nassimi, A.; Bonella, S.; Kapral, R. Analysis of the Quantum-Classical Liouville Equation in the Mapping Basis. *J. Chem. Phys.* **2010**, *133*, 134115.

(71) Kim, H. W.; Rhee, Y. M. Improving Long Time Behavior of Poisson Bracket Mapping Equation: A Non-Hamiltonian Approach. *J. Chem. Phys.* **2014**, *140*, 184106.

(72) Miller, W. H.; Cotton, S. J. Classical Molecular Dynamics Simulation of Electronically Non-Adiabatic Processes. *Faraday Discuss.* **2016**, *195*, 9−30.

(73) Cotton, S. J.; Miller, W. H. Symmetrical Windowing for Quantum States in Quasi-Classical Trajectory Simulations. *J. Phys. Chem. A* **2013**, *117*, 7190−7194.

(74) Cotton, S. J.; Igumenshchev, K.; Miller, W. H. Symmetrical Windowing for Quantum States in Quasi-Classical Trajectory Simulations: Application to Electron Transfer. *J. Chem. Phys.* **2014**, *141*, 084104.

(75) Cotton, S. J.; Miller, W. H. A Symmetrical Quasi-Classical Spin-Mapping Model for the Electronic Degrees of Freedom in Non-Adiabatic Processes. *J. Phys. Chem. A* **2015**, *119*, 12138−12145.

(76) Cotton, S. J.; Miller, W. H. The Symmetrical Quasi-Classical Model for Electronically Non-Adiabatic Processes Applied to Energy Transfer Dynamics in Site-Exciton Models of Light-Harvesting Complexes. *J. Chem. Theory Comput.* **2016**, *12*, 983−991.

(77) Miller, W. H.; Cotton, S. J. Communication: Wigner Functions in Action-Angle Variables, Bohr-Sommerfeld Quantization, the Heisenberg Correspondence Principle, and a Symmetrical Quasi-Classical Approach to the Full Electronic Density Matrix. *J. Chem. Phys.* **2016**, *145*, 081102.

(78) Cotton, S. J.; Liang, R.; Miller, W. H. On the Adiabatic Representation of Meyer-Miller Electronic-Nuclear Dynamics. *J. Chem. Phys.* **2017**, *147*, 064112.

(79) Meyer, H. D.; Miller, W. H. A Classical Analog for Electronic Degrees of Freedom in Nonadiabatic Collision Processes. *J. Chem. Phys.* **1979**, *70*, 3214−3223.

(80) Cotton, S. J.; Miller, W. H. Symmetrical Windowing for Quantum States in Quasi-Classical Trajectory Simulations: Application to Electronically Non-Adiabatic Processes. *J. Chem. Phys.* **2013**, *139*, 234112.

(81) Miller, W. H.; Cotton, S. J. Communication: Note on Detailed Balance in Symmetrical Quasi-Classical Models for Electronically Non-Adiabatic Dynamics. *J. Chem. Phys.* **2015**, *142*, 131103.

(82) Bellonzi, N.; Jain, A.; Subotnik, J. E. An Assessment of Mean-Field Mixed Semiclassical Approaches: Equilibrium Populations and Algorithm Stability. *J. Chem. Phys.* **2016**, *144*, 154110.

(83) Wu, J.; Cao, J. S. Linear and Nonlinear Response Functions of the Morse Oscillator: Classical Divergence and the Uncertainty Principle. *J. Chem. Phys.* **2001**, *115*, 5381.

(84) Kryvohuz, M.; Cao, J. Quantum-Classical Correspondence in Response Theory. *Phys. Rev. Lett.* **2005**, *95*, 180405.

(85) López-López, S.; Martinazzo, R.; Nest, M. Benchmark Calculations for Dissipative Dynamics of a System Coupled to an Anharmonic Bath with the Multiconfiguration Time-Dependent Hartree Method. *J. Chem. Phys.* **2011**, *134*, 094102.

(86) Stock, G.; Thoss, M. Semiclassical Description of Nonadiabatic Quantum Dynamics. *Phys. Rev. Lett.* **1997**, *78*, 578−581.

(87) Miller, W. H. The Semiclassical Initial Value Representation: A Potentially Practical Way for Adding Quantum Effects to Classical Molecular Dynamics Simulations. *J. Phys. Chem. A* **2001**, *105*, 2942−2955.

(88) Ananth, N.; Venkataraman, C.; Miller, W. H. Semiclassical Description of Electronically Nonadiabatic Dynamics via the Initial Value Representation. *J. Chem. Phys.* **2007**, *127*, 084114.

(89) Kelly, A.; van Zon, R.; Schofield, J.; Kapral, R. Mapping Quantum-Classical Liouville Equation: Projectors and Trajectories. *J. Chem. Phys.* **2012**, *136*, 084101.

(90) Thompson, K.; Makri, N. Influence Functionals with Semi-classical Propagators in Combined Forward-Backward Time. *J. Chem. Phys.* **1999**, *110*, 1343.

(91) Wan, C.; Schofield, J. Exact and Asymptotic Solutions of the Mixed Quantum-Classical Liouville Equation. *J. Chem. Phys.* **2000**, *112*, 4447−4459.

(92) Martinez, F.; Hanna, G. Mixed Quantum-Classical Simulations of Transient Absorption Pump−Probe Signals for a Photo-Induced Electron Transfer Reaction Coupled to an Inner-Sphere Vibrational Mode. *J. Phys. Chem. A* **2016**, *120*, 3196−3205.